AIAA JOURNAL
Vol. 45, No. 1, January 2007

Separation Control by Self-Activated Movable Flaps

Robert Meyer,* Wolfram Hage,† and Dietrich W. Bechert‡
German Aerospace Center (DLR), 10623 Berlin, Germany
and
Markus Schatz,§ Thilo Knacke,¶ and Frank Thiele**
Technical University of Berlin, 10623 Berlin, Germany

DOI: 10.2514/1.23507

Separation control is an important issue in the physiology of birdflight. Here, the adaption of the separation control mechanism by bird feathers to the requirements of engineering applications is described in detail. Self-activated movable flaps similar to artificial bird feathers represent a high-lift system for increasing the maximum lift of airfoils. Their effect on the unsteady flow around a two-dimensional airfoil configuration is investigated by a joint numerical and experimental study. First, attention is paid to the automatic opening and closing mechanism of the flap. Following this, its beneficial effect on lift is investigated for varying incidences and flap configurations. In-depth analysis of experimental and numerical results provides a detailed description of the important phenomena and the effect of self-adjusting flaps on the flow around the airfoil. In the second part of this paper, a contribution is made to verification of the applicability of unsteady Reynolds-averaged approaches using statistical turbulence models for unsteady flows with particular attention to turbulent time scales with comparison to the results of a hybrid simulation based on unsteady Reynolds-averaged Navier–Stokes equations and large-eddy simulation. Finally, flight experiments are described using an aircraft with movable flaps fitted on its laminar wing.

Nomenclature

A	=	amplitude of oscillation
b	=	wing span
c	=	chord length
c_F	=	flap-moment coefficient
c_G	=	gravity-moment coefficient
c_L; c_D	=	lift and drag coefficients
c_R	=	reverse flow parameter
k	=	turbulent kinetic energy
Lt	=	turbulent length scale
l_F	=	flap length
M_F	=	flap moment due to fluid force
M_G	=	flap moment due to gravity
Re	=	Reynolds number based on chord length
Sr	=	Strouhal number based on flap length
u_0	=	inflow velocity
x_d	=	detachment position
α	=	angle of attack
β, $\beta_{\max}$	=	flap deflection angle, maximum angle
γ	=	conventional flap angle
ρ	=	density
ω	=	specific turbulent dissipation

Presented as Paper 1243 at the 42nd AIAA Aerospace Sciences Meeting and Exhibit, Reno, Nevada, 5–8 January 2004; received 2 March 2006; revision received 5 September 2006; accepted for publication 5 September 2006. Copyright © 2006 by the authors. Published by the American Institute of Aeronautics and Astronautics, Inc., with permission. Copies of this paper may be made for personal or internal use, on condition that the copier pay the $10.00 per-copy fee to the Copyright Clearance Center, Inc., 222 Rosewood Drive, Danvers, MA 01923; include the code $10.00 in correspondence with the CCC.

*Research Scientist, Department of Engine Acoustics, Mueller-Breslau-Strasse 8.
†Research Scientist, Department of Engine Acoustics, Mueller-Breslau-Strasse 8.
‡Research Scientist, Department of Engine Acoustics, Mueller-Breslau-Strasse 8. Senior Member AIAA (Deceased).
§Research Scientist, Institute of Fluid Dynamics and Technical Acoustics, Mueller-Breslau-Strasse 8. Member AIAA.
¶Research Scientist, Institute of Fluid Dynamics and Technical Acoustics, Mueller-Breslau-Strasse 8.
**Professor, Institute of Fluid Dynamics and Technical Acoustics, Mueller-Breslau-Strasse 8. Member AIAA.

I. Introduction

BIRDS have a very effective means of dealing with flow separation on their wings. Once attention has been drawn to it, it is comparatively easy to observe on almost any bird: During the landing approach or in gusty winds, the feathers on the upper surface of bird wings tend to pop up (Fig. 1).

Liebe interpreted this behavior as a biological high-lift device [1]. It seemed a likely supposition that *flow separation* could be delayed, with *higher lift* allowing *lower flight speeds*. He suggested the adoption of the same principle to an engineering application. At the former German Aeronautical Establishment (DVL) flight experiments with a Messerschmitt Me 109 fighter airplane were carried out as early as 1938. A piece of leather was attached to the upper side of one wing. The ensuing aerodynamic asymmetry of the wings caused the aircraft to be difficult to handle, particularly at high angles of attack. The problems occurring in this initial test prevented further investigation of the concept. Liebe's original idea was that once separation starts to develop on a wing, reversed flow is bound to occur in the separation regime [1]. Under these locally reversed flow conditions, light feathers would pop up, acting like a brake on the spreading of flow separation toward the leading edge. Liebe was aware of the fact that flow separation is often three dimensional with variable patterns in the spanwise direction. Thus, he considered it essential to be able to interact locally with separation regimes (Fig. 1). Following Liebe's ideas, a few tentative flight experiments have been carried out with small movable plastic sheets installed on a glider wing on the upper surface near the trailing edge. A slightly augmented behavior of the glider aircraft at high angles of attack was reported [2].

However, the first truly successful application followed in the 1990s with flaps on an airfoil in a wind tunnel. These experiments of Patone and Mueller [3] demonstrated the beneficial effect of free-movable flaps for low Reynolds numbers ($Re < 150.000$). Bechert et al. [4,5] and Meyer [6] extended the investigations to a typical glider Reynolds number of $Re = 10^6$. The desirable behavior of self-activated flaps at different angles of attack is shown in Fig. 2. At low incidence, the flap remains attached to the airfoil surface and does not have any effect on the aerodynamics. However, with increasing angle of attack when flow separation in the trailing edge region occurs, the flap lifts and self-adjusts to a position dependent on the aerodynamic forces and flap weight.

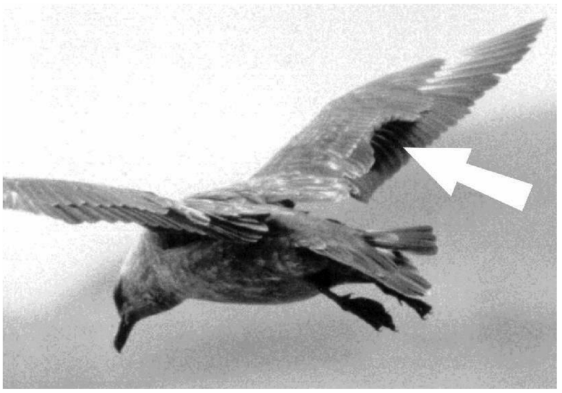

Fig. 1 A bird's wing with popped up feathers to prevent further proliferation of flow separation (photo by I. Rechenberg).

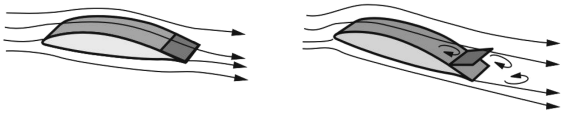

Fig. 2 The self-adjusting flap is closed at low angle of attack and pops up automatically at higher angles.

Self-activated flaps are a tool for passive flow control, meaning that no external energy is required by the control mechanism. The opening and closing mechanism is activated by the mean flow itself. Compared to active flow control devices such as periodic suction and blowing or driven flap oscillations, the present approach forms a simple and cost-effective tool that promises to improve the performance of high-lift devices.

The goal of the present investigation is to provide a detailed description of the relevant flow physics for self-adjusting movable flaps on airfoils. Initially, wind tunnel experiments were performed to obtain an overview of the general behavior and to set a proper flap design for the following more detailed experimental and numerical investigations. The combined analysis of both experimentally and numerically obtained results can provide a continuative understanding of the behavior of free-movable flaps and the unsteady flowfield. Particular attention is also given to the issue of applying unsteady Reynolds-averaged simulations (URANS) to highly unsteady flow phenomena. Most of the numerical simulations are based on the Reynolds-averaged approach. An associated goal is to verify the applicability of statistical turbulence models for this kind of flow and to prove that all important flow features can be captured by a comparison to the results of the hybrid URANS/LES (large-eddy simulation) approach. Finally, movable flaps were installed on a glider plane for free-flight testing.

II. Experimental Investigation

An initial experimental investigation forming part of a previous study [4] was carried out with part of a full-scale wing section of the motor glider Stemme S10 in a wind tunnel. Lift and drag were measured using a balance. The flow in the experimental test section is almost 2-D. A detailed description of the 2-D-test section can be found in [6]. The Reynolds number was between $1 \times 10^6 < Re < 2 \times 10^6$, to simulate flight Reynolds numbers. This particular regime is relevant for the high-lift condition under consideration. All investigations have been performed in the low-speed wind tunnel of the Institute of Fluid Dynamics and Technical Acoustics (former Hermann-Foettinger-Institute for Fluid Mechanics) at the Technical University Berlin.

A. Movable Flaps on Wings: Artificial Bird Feathers

In initial wind tunnel trials, it emerged that the naive approach of emulating bird feathers by simply attaching multiple plastic strips to the wing surface produced rather confusing results. Some strips tend to pop up randomly and also the lift increase was not permanent.

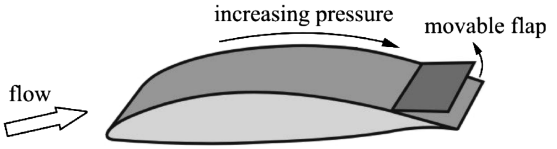

Fig. 3 HQ17 wing section with movable flap.

Therefore, the experiments were continued with a simpler device, that is, a thin movable flap on the upper surface of a glider airfoil. The flaps used consisted either of flexible plastic material or thin sheet metal. The flaps were attached to the rear part of the airfoil and could pivot on their leading edges (Fig. 3).

Under attached flow conditions, the movable flap is very slightly raised. This is due to the fact that the static pressure increases in the downstream direction in the rear part of the upper surface of the airfoil. Thus, the space under the flap is connected to a regime of slightly elevated static pressure. Consequently, in most places, the pressure beneath the movable flap is higher than above it. This behavior turns out to be not at all advantageous. The drag is slightly increased due to the small separation regime at the end of the flap. In addition, there is a slight decrease in lift, because the angle of the airfoil skeleton line at the trailing edge is decreased and the effective angle of attack of the airfoil is also decreased. Consequently, for attached flows, the impact of the movable flap is a slightly detrimental one. However, there are several ways to deal with this problem. The first and most obvious possibility would be to lock the movable flap onto the airfoil surface under attached flow conditions. The second is also rather simple: The flap could be made porous in order to obtain equal static pressure on both sides of the flap under attached flow conditions. A third method is to make the trailing edge of the flap jagged, as can be seen in Fig. 4. This also gives rise to an exchange of pressures. Incidentally, the latter two modifications are in fact characteristic of bird wings.

Now, how do the movable flaps respond to reversed flow? First, it should be mentioned that the velocities in the reversed flow region

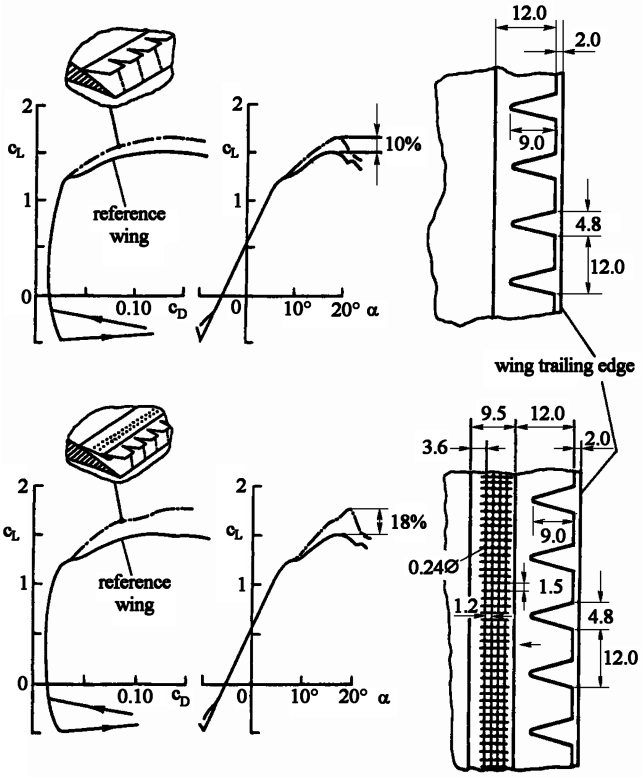

Fig. 4 Experimental data of different variants of movable flaps installed on a laminar glider airfoil. Top: single jagged flap; bottom: double flap, with a porosity of 1–2% in the front part (all numbers give percentage of airfoil chord).

are considerably smaller than the mean flow velocity. Thus, the movable flaps must be very light and should respond with high sensitivity to even weak reversed flows. A very soft trailing edge of the movable flaps facilitates such a sensitive response. Again, this feature is evident with bird feathers. Once the flow starts to separate, the movable flap follows gradually. It does not, however, protrude into the high-speed flow above the separation wake. This high-speed flow would push the flap back to a lower elevation. It is useful to stress the marked difference between the movable flaps and a conventional rigid spoiler on a wing [7]: A spoiler protrudes into the high-speed flow regime and increases the width of the wake. In this way, it increases the drag and reduces the lift. By contrast, at high angles of attack, the movable flap has the opposite effect, that is, reducing drag and increasing lift. At the same time, the effective shape of the airfoil changes due to the slightly elevated flap and a lower effective angle of attack ensues. Thus, the pressure distribution on the airfoil is adjusted in such a way that the tendency for flow separation is reduced. Consequently, the flow remains attached up to higher angles of attack and the lift of the wing is increased.

Nevertheless, there are limits for everything. At very high angles of attack, the reversed flow causes the flap to tip forward entirely and the effect of the flap would disappear. That, however, can be prevented by limiting the opening angle of the flap. Very simply, this is achieved by attaching limiting strings to the movable flap. The optimal maximum opening angle of the flaps was determined experimentally. It was found to lie between 60 deg (for solid and porous flaps) and about 90 deg (for flaps with jagged trailing edges) [6]. Once the full opening angle is reached, the separation jumps forward over the flap. Hence, for very high angles of attack, the effect of the movable flap finally decreases and vanishes. On birds, tipping over of the feathers is not observed. The feather shafts are sufficiently stiff and well anchored to prevent this detrimental occurrence.

B. Parameters for Flap Design Optimization

An important question concerns the location on the airfoil where a movable flap should be installed. The experiments started with movable flaps located at the upper downstream end of the airfoil. This appeared reasonable, because on laminar airfoils, the first 60–70% of the upper surface is designed to remain laminar. Any attachment or other deviation from a perfectly smooth surface in this laminar regime would cause transition, producing significant additional drag. On bird wings which operate at lower Reynolds numbers, however, surface smoothness is less important. By contrast, on the rear part of the airfoil and downstream of the laminar regime, minor changes in the surface quality do not produce a detectable increase of the drag. It was found in the experiments that the trailing edge of the movable flap should be located slightly upstream ($\geq$ 1% chord) of the trailing edge of the airfoil, otherwise it would not respond properly to flow separation. On the other hand, the farther upstream the flap is located, the farther upstream the flow separation would have to have already spread before the flap starts to respond. Thus, if influence of incipient separation is desired, the trailing edge of the flap should be located close to the trailing edge of the airfoil.

Another intriguing question involves the size of a movable flap. The wind tunnel experiments started with comparatively small flaps having a length of about 12% of the airfoil chord length [4,6]. The effect was significant (Fig. 4) and resulted in a 10% increase of maximum lift. Increasing the flap length produced a further increase of maximum lift. For instance, a flap length of 22% resulted in an increase of 18% of the maximum lift. However, for large movable flaps (which are not flexible), the self-adjustment to the flow situation becomes less satisfactory. Typically, a movable flap starts to rise when the flow separation has already reached its upstream edge. On the other hand, full reattachment of the flap is obtained at a lowered angle of attack when the reattachment line of a reference wing (without movable flap) has moved downstream to the location of the flap trailing edge. That creates a significantly different behavior for increasing angles as compared with decreasing angles. This hysteresis in the airfoil data is not desired because it would make an aircraft difficult to handle. One way to avoid this problem is to divide the flap into movable parts attached to each other. A porosity of just 1–2% of the front part is also helpful. Indeed, this double flap (Fig. 4, bottom) adjusts itself much better and the hysteresis is practically eliminated. Nevertheless, the impressive increase in maximum lift is still maintained.

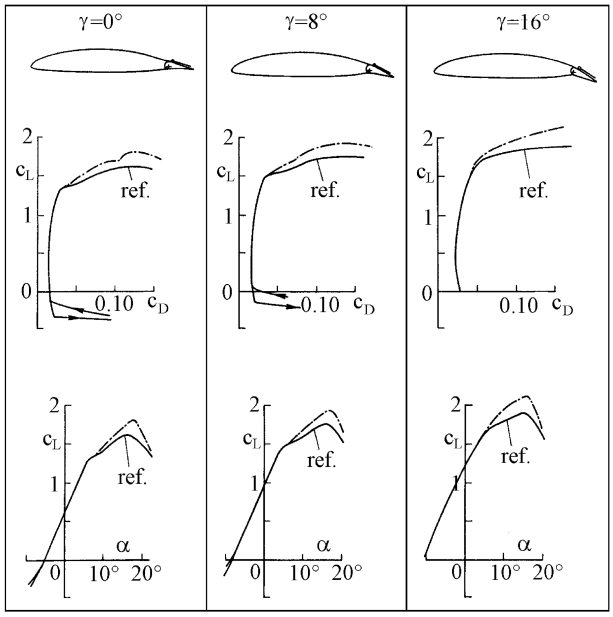

Fig. 5 Experimental data of the combination of conventional and movable flaps for three different flap angles γ. Dotted curves: with movable flap.

As a specific preparation for flight experiments, we made sure that our movable flaps would also work properly in combination with the conventional flaps on the wings. Figure 5 shows data with both types of flaps combined. The movable flap is actually mounted on the conventional flap. As can be seen in Fig. 5, the increase of lift caused by the movable flap persists.

From these fundamental investigations, an optimum flap configuration exhibiting high reliability and freedom from hysteresis was identified. The configuration airfoil is a HQ17 of Horstmann and Quast [8] at a Reynolds number of $Re = 10^6$ and a wide range of incidence. The flap is mounted on the airfoil at $x/c = 0.8$ via a free-moving hinge. The maximum flap angle is, however, constrained to 57 deg. The main body of the flap is constructed from an aluminum sheet, with the trailing edge made of flexible plastic film (Fig. 8). This configuration forms the base of the current, more detailed experimental and numerical investigations. In the experimental work, pressure distributions as well as separation positions and transition locations have been measured. A description of the numerical simulations now follows.

III. Numerical Method

The applied numerical code ELAN, of the Technical University Berlin, is based on a three-dimensional incompressible finite-volume scheme to solve the Navier–Stokes equations. The method is fully implicit and of second order in space and time. Based on the semi-implicit method for pressure-linked equations pressure correction algorithm, a colocated storage arrangement for all quantities is applied. Convective fluxes are approximated by a total variation diminishing—monotone upstream-centered scheme for conservation laws scheme.

A. Turbulence Modeling

The simulation program can be run in an URANS mode, solving the unsteady Reynolds-averaged Navier–Stokes equations using statistical turbulence models as well as in a mode for LES or combinations of both. In simulations of unsteady turbulent flows by Reynolds-averaged approaches, the treatment of turbulent time

scales always requires special attention. An important assumption in the derivation of statistical turbulence models is that time averaging can be used instead of ensemble averaging.

Therefore the applicability of these models depends on the existence of a *spectral gap* of one or two orders between the resolved time scales and the modeled scales. Otherwise a formal conflict can arise from an overlapping of resolved and modeled motions. The turbulence model will transfer energy from the large-scale motion into dissipation, but simple URANS models cannot provide a counteracting mechanism (*backscatter*). As the occurring turbulent time scales are not known in advance, the entire flowfield needs to be checked for the smallest ratio between resolved and modeled time scales. The resolved time scales of the large-scale motions have to be significantly larger than the high frequency small-scale motions that are captured by the turbulence model. Problems can occur if parts of the spectrum are modeled as well as resolved. In previous URANS investigations with a large variety of different one- and two-equation turbulence models as well as explicit algebraic Reynolds stress models (EARSM), the linear local realizable (LLR) k–ω model by Rung [9] exhibited the best overall performance for the present case [10]. It is an improved two-equation eddy-viscosity model with particular attention to the realizability conditions.

Additionally, hybrid URANS/LES simulations are performed which are also based on Rung's LLR k–ω model. In the transport equation for the turbulent kinetic energy k, the destruction term is replaced by a formulation based on the turbulent length scale L_t:

$$\frac{D_{\rho k}}{D_t} - \mathrm{Diff}(\rho \cdot k) = \rho \cdot Prod(k) - \rho \cdot \underbrace{\beta_k \cdot \frac{k^{3/2}}{L_t}}_{\mathrm{Diss}(k)} \tag{1}$$

This turbulent length scale is used to switch between the *URANS* and the *LES* mode, similar to the concept of *detached-eddy simulation (DES)* [11]:

$$L_t = \min(L_{t,\mathrm{URANS}}, L_{t,\mathrm{LES}}) = \min\left(\frac{\sqrt{k}}{c_\mu \omega}, C_{\mathrm{DES}}\Delta\right) \tag{2}$$

with the specific dissipation $\omega = k/\varepsilon$ and c_μ is the anisotropy parameter in the LLR model and is not constant. In the LES mode, the length scale $L_{t,\mathrm{LES}}$ is given by the definition of Strelets [12] with the constant $C_{\mathrm{DES}} = 0.78$ and using the local resolution of the mesh: $\Delta = \max(\Delta x, \Delta y, \Delta z)$.

B. Transition

The investigated HQ17 airfoil is a laminar airfoil. As laminar flow stretches over large parts of the airfoil, a proper prediction of transition plays an important role for a suitable computational representation of the flow. Therefore transition is fixed by an iterative procedure based on the detection of laminar separation [10].

For the clean airfoil case, transition locations on the suction side have been measured by flow visualization with a mixture of oil and titanium dioxide. Comparison of measured and predicted transition locations indicate that this procedure can be successfully applied to this kind of flow (Fig. 6). In the laminar region the source terms in the turbulence model are switched off and the free-flow conditions are transported until the transition location.

C. Computational Mesh

The computational c-type mesh provides 202 chordwise cells around the main airfoil and 196 around the flap resulting in 37,000 cells in total for the 2-D case. In the three-dimensional simulation the mesh consists of 30 layers in the z direction covering a span of $b = 0.18c$ and has about 1×10^6 nodes.

The nondimensional wall distance of the first cell center remains below $Y^+ = 1$ on the complete surface for an attached steady case with the exception of the flap upper surface with $Y^+ < 2.5$ due to restrictions of the mesh topology (downstream "P" in Fig. 7). The

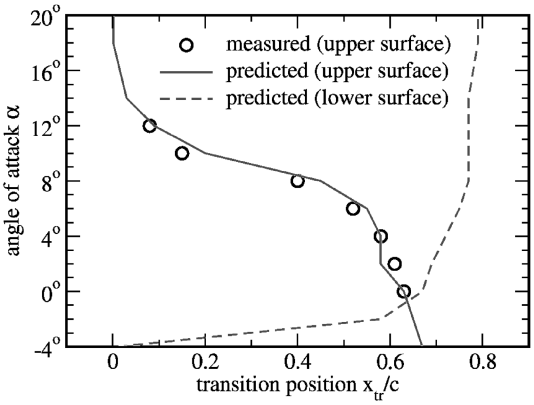

Fig. 6 Measured and predicted transition location for the clean HQ17 laminar profile at $Re = 10^6$.

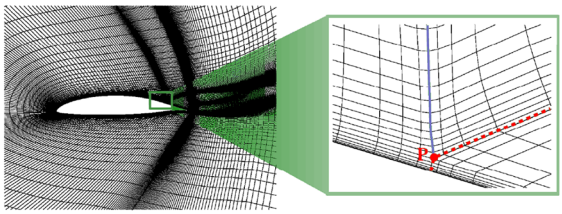

Fig. 7 Computational mesh that represents the clean HQ17 airfoil as well as a configuration of airfoil and flap.

mesh can represent the clean HQ17 airfoil if the dashed line forms a block interface or a configuration with a flap if the dashed line is modeled as a solid wall. The computational domain covers six chords upstream and 10 chords downstream of the configuration. Additional simulations use a 137,000 cells mesh to evaluate mesh dependency in the 2-D case and another mesh covering one chord length in the spanwise direction ($b = c$) in the 3-D case.

D. Flap Motion

The flap is modeled as a solid body and has only 1 degree of freedom, the flap deflection angle $\Delta\beta$. The flap motion is then governed by a balance of moments around the hinge center S (Fig. 8):

$$\theta_S = \frac{d^2 \cdot \beta}{dt^2} = -M_F(t) - M_G(t) \tag{3}$$

θ_S is the moment of inertia, $M_G(t)$ is a moment caused by the flap weight, and $M_F(t)$ is a moment caused by the fluid forces on the flap. Both moments can be represented by nondimensional coefficients c_G and c_F. $M_F(t)$ is mainly given by the difference between the static pressure at the upper flap surface (p_u in Fig. 8) and the lower flap surface (p_l):

$$c_F = \frac{M_F}{(1/2)\rho c u_0^2 c b} = 2\int_{r=0}^{l_F} \frac{r(p_u - p_l)}{\rho c^2 u_0^2}\,\mathrm{d}r \tag{4}$$

Equation (3) can be discretized by a second order finite-difference approach and is solved numerically in a loose coupled system

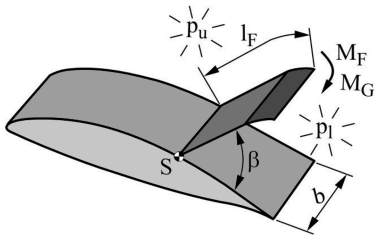

Fig. 8 Sketch of the computational model for the motion of self-adjusting flaps.

together with the flowfield. The flexible flap trailing edge is captured by the assumption that it will always adjust in the mean flow direction.

To capture the geometry in the case of a moving flap, the numerical grid needs to be distortable. Starting with a basic mesh at a low flap angle the mesh around the upward-deflecting flap is deformed using Wick's method based on an analogy with structural mechanics [13] for each time step. If necessary, a biharmonic smoothing algorithm is applied to improve the mesh quality. This procedure allows simulations for flap deflection angles in the range of $\beta = 14$ deg to 68 deg.

E. Numerical Results

This paragraph is divided into simulations of a flap at fixed deflection angle (static flap) and a second section considering a free-movable flap in which the fluid-structure interaction is simulated. The investigations of the static flap cases cover two- and three-dimensional approaches. To avoid shortcomings from too simple turbulence modeling for two cases, DES simulations have been performed and finally the flap mass is varied to study one important parameter governing the opening and closing of the flap. From initial numerical investigations of the clean airfoil, it was known that the flow becomes unsteady at high angles of attack and vortex shedding occurs. Therefore all computations are unsteady with a typical time step of $\Delta t = 0.01c/u_0$. For detailed information about the flow around the HQ17 reference profile see Schatz [10].

1. *Static Flap*

The first step of modeling free-movable flaps is to run a series of simulations with a static flap at different deflection angles and angles of attack. The analysis of these computations allows the identification of one flap position for each angle of attack where the flap moment M_F and the gravity moment M_G are balanced ($c_F = -c_G$). This equilibrium position should correspond to the mean location of a self-adjusting flap. In Fig. 9 the resulting flap coefficient c_F is plotted for different flap angles and incidences. Positive quantities mean that the flap is pushed downward by the fluid and in the case of negative c_F it will pop up.

For further analysis, isosurfaces of the mean flow velocity in the x direction are plotted in Fig. 10. The edge of the reverse flow region ($u = 0$) is marked by a black line. It is found that an optimum angle β is achieved when the flap just slightly touches the detached shear layer. In the case of lower flap angles, the flap remains inside the reverse flow region which it splits into two parts. For the mean lift, however, it shows less effect (right column of Fig. 10). In the case of excessive angles, the flap works like a spoiler and generates additional drag (left column of Fig. 10).

The unsteady flow in the wake can be stabilized by flaps at low flap angles and at the same time the size of detaching vortices as well as the amplitude of lift oscillations decreases. This effect is comparable to that of a splitter plate [14,15] in the wake of cylinders. For each flap deflection angle β, a lift polar with the typical shape is computed. With increasing flap deflection the camber ratio of the configuration decreases and the polar is shifted to the right (this behavior makes

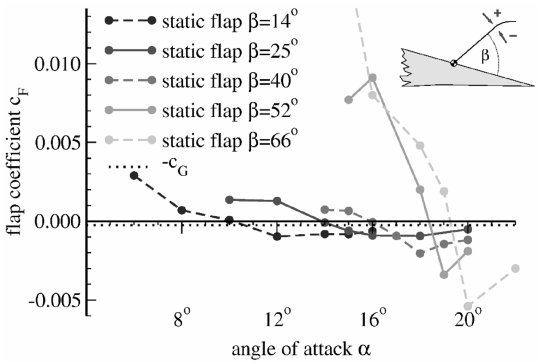

Fig. 9 Flap coefficient c_F for varying deflection angle β.

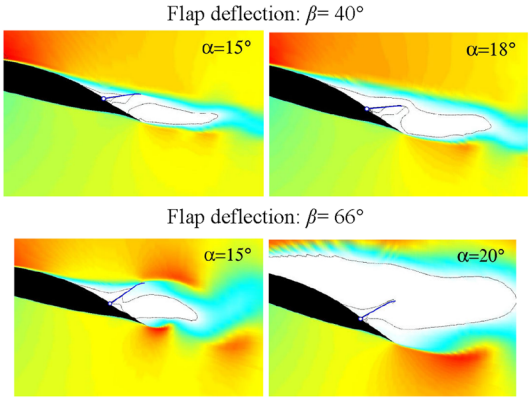

Fig. 10 Mean flow velocity in the x direction. Rows: different flap deflection β; columns: different angle of attack; left: excessive flap deflection; right: insufficient flap deflection.

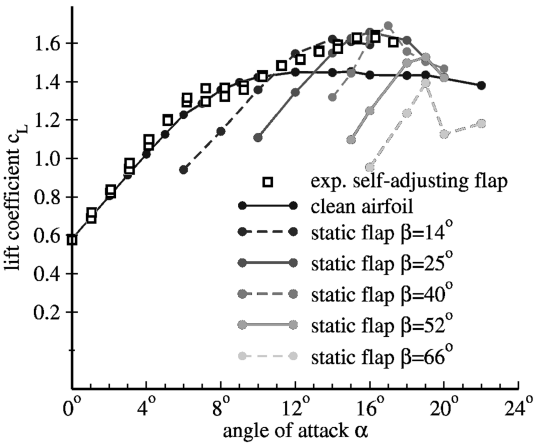

Fig. 11 Lift coefficient for the HQ17 airfoil with static flap at different deflection angle β.

spoilers a very effective tool for the destruction of lift). As each of these polars exceeds the reference wing in a particular region of incidence, higher lift coefficients are shown to be possible (Fig. 11). The envelope curve of all polars, representing the maximum achievable lift by static flaps, promises a gain in lift of up to 18%. In the equilibrium position, however, the lift remains below this maximum and a gain of only about 15% can be observed (Fig. 17). These results match almost perfectly with the experimental wind tunnel results.

At the same time the flow detachment from the airfoil upper surface can be delayed by the flap. Figure 12 shows that between $\alpha = 10$ deg and $\alpha = 20$ deg, the flow is able to remain attached longer than in the reference airfoil case. Here the numerical

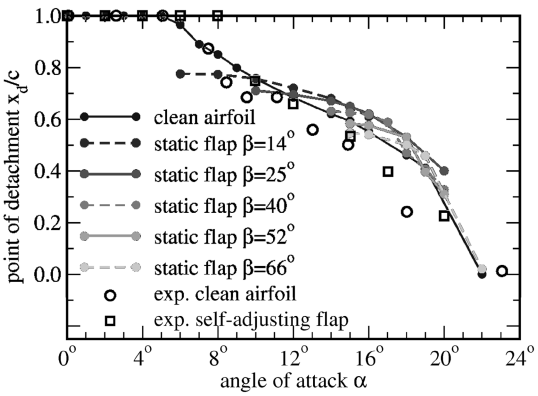

Fig. 12 Point of flow detachment for the HQ17 airfoil with static flap and ranging deflection.

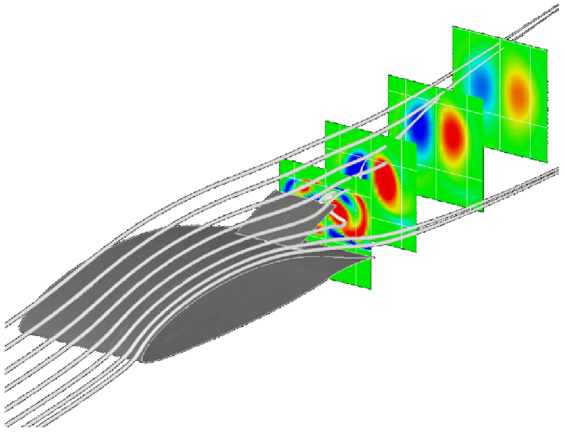

Fig. 13 Streamlines of the flowfield around a static flap at high flap deflection angle ($\beta = 40$ deg) at an airfoil at low angle of attack ($\alpha = 4$ deg).

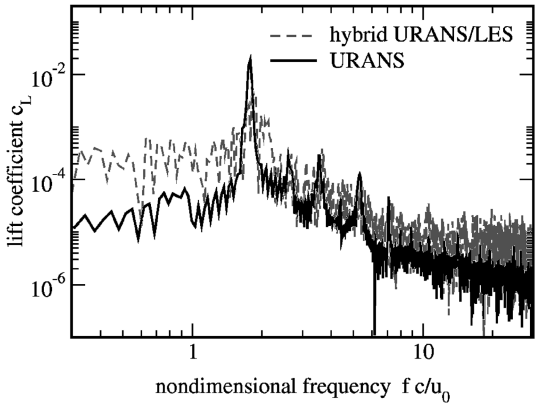

Fig. 14 Frequency spectrum of lift for URANS and the hybrid URANS/LES method for the flow around an airfoil with static flap. ($\alpha = 16$ deg, $\beta = 40$ deg).

simulations exhibit the same quantitative effect of the flap like the experiments, where flow separation is detected by flow visualization with a mixture of oil and titanium dioxide. However, a constant shift between the experimental and numerical results is observed.

For the next step the numerical investigations are extended to the three-dimensional case. First the clean airfoil is simulated and, following this, an airfoil with a flap that covers the complete span. The three-dimensional simulations indicate that the flow remains two dimensional as long as the geometry is two dimensional. The mean flow quantities show almost no three dimensionality (not plotted).

Finally, a flap extending over only part of the wing span is computed. For low angle of attack ($\alpha = 4$ deg) and large flap deflection ($\beta = 40$ deg), the effect is comparable to a spoiler and causes strong perturbations in the flow, in particular, two vortices are generated at the edges of the flap. The lift of the wing can be completely destroyed by the flap (Fig. 13).

In the case of a flap in an equilibrium position, however, the effect of the flap edges on the flow is minor. As the boundary layer on the flap surface and the free shear layer in the spanwise location without flap are very similar, almost no interaction of the flapped and the clean part of the wing can be observed. In this case no significant effect of the flap edge on the opening mechanism of the flap is apparent because almost no fluid forces are acting on the flap ($c_F < 10^{-3}$). Separation is delayed, the lift can be enhanced by the flap, and all aerodynamic forces are comparable to the infinite flap case. Figure 15 gives an impression of the flow around a flap covering part of the wing span.

2. *Hybrid URANS/LES Computations*

According to the problem of resolving time scales additional hybrid URANS/LES computations have been performed. Hybrid URANS/LES results obtained on the same numerical mesh with the same time step can be compared to the URANS computations. Both methods give similar mean aerodynamic forces. The unsteady features of the flow can be compared by a spectrum of lift in Fig. 14. One dominant peak corresponding to the same shedding frequency can be identified in the results of both methods. However, in the hybrid URANS/LES simulation the level of lift fluctuation beside this peak is 3–10 times higher than in the Reynolds-averaged method especially for lower frequencies. In Fig. 15, isosurfaces of the w velocity and contours of eddy viscosity for the hybrid approach results of the case of a wing with a $b/c = 10\%$ flap are presented for $\alpha = 16$ deg angle of attack. Here the enhanced resolution of small-scale unsteady flow structures with the hybrid approach is visible. In the time-averaged quantities, however, the flowfield does not show significant differences compared to URANS (not plotted).

3. *Freely Movable Flap*

In the present investigations the flap motion is modeled by a coupled fluid-structure interaction method always starting from the

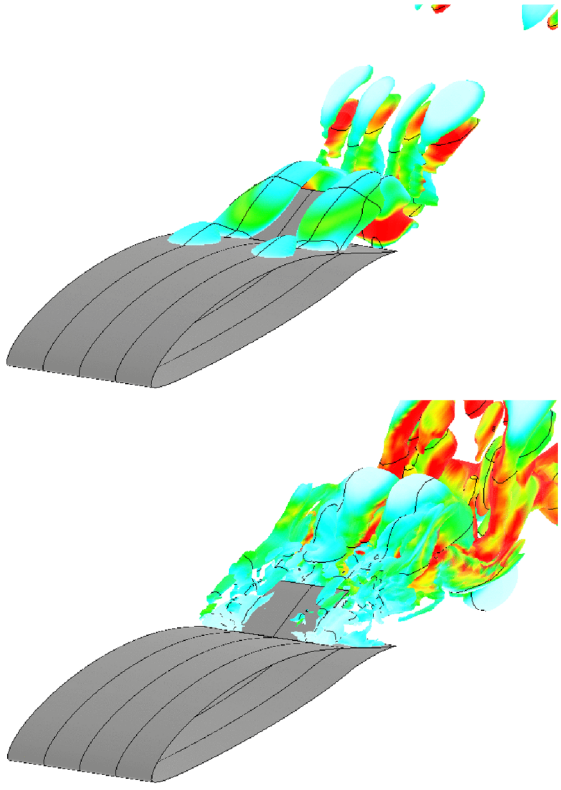

Fig. 15 Isosurfaces of the spanwise velocity colored by contours of turbulent viscosity of the hybrid URANS/LES approach (flow around static flap). Upper figure: URANS results (dark corresponds to $\nu_t = 1000\nu$); lower figure: results of hybrid approach (dark corresponds to $\nu_t = 200\nu$).

equilibrium flap deflection determined for the static flap. It was seen that the flap finds this equilibrium position by itself, and furthermore, this position is stable. The lift coefficient is augmented by the deployment of the flap and can be increased by 12.9% compared to the clean airfoil (Fig. 16). At high angles of attack, the flowfield is dominated by flow separation. In the range of incidence when the self-adjusting flap is active, the detachment can be significantly delayed (Fig. 17). These numerical results are qualitatively in good agreement with the experimental data although a significant shift between measured and computed separation locations occurs for the whole range of incidences.

In the URANS computations, the flowfield in the wake is dominated by a single fluctuation frequency. Based on the flap length, it corresponds to a nondimensional Strouhal number which is plotted in Fig. 18. The Strouhal number for the self-adjusting flap is slightly higher compared to that of the clean airfoil, but no difference

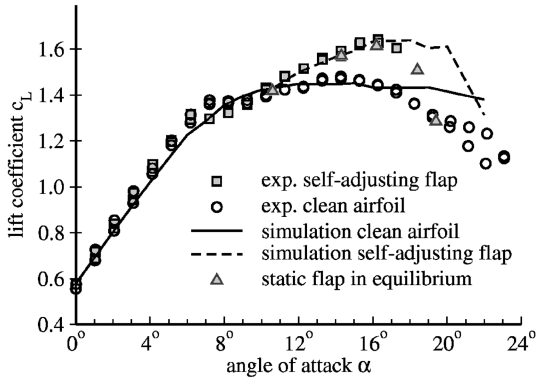

Fig. 16 Lift coefficient for the HQ17 airfoil with self-adjusting flap.

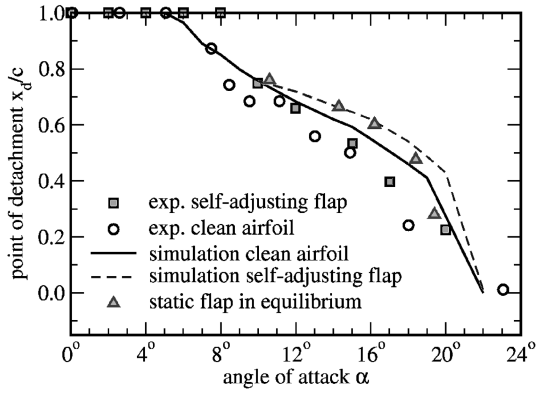

Fig. 17 Point of flow detachment for the HQ17 airfoil with self-adjusting flap.

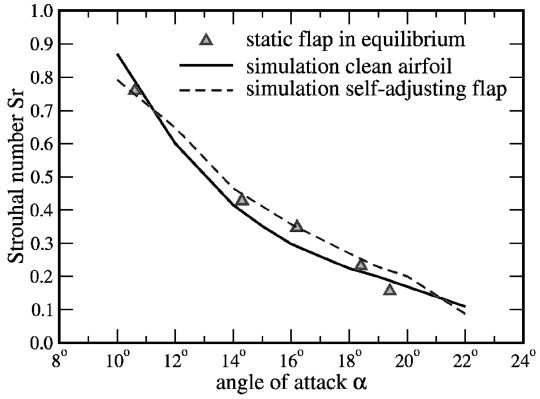

Fig. 18 Strouhal number for different angles of attack.

to the static flap is visible. The flap also has a stabilizing effect on the turbulent wake. The mean deflection angle differs from the equilibrium position of the static flap, and as Fig. 19 shows, it is slightly lower than that observed in the experiments. Because of the relatively crude modeling of the flap-tip shape, all deflection angles are slightly underpredicted in the computations. The numerical simulation provides the possibility of quantification of the intensity of the backflow in the reverse flow region. The nondimensional reverse flow factor c_R is defined by

$$c_R = \frac{\dot{m}_R}{\dot{m}_0} = \frac{1}{\rho c^2 u_0} \int_{y=0}^{y(u=0)} \rho u_i \, \mathrm{d}A_i \tag{5}$$

This factor is computed for the clean airfoil and the airfoil with a self-adjusting flap. Figure 20 shows that over a wide range of incidence, the reverse mass flow can be significantly reduced by the flap. One important effect is based on the division of the separated flow region into two parts, with much lower intensity than in the clean airfoil case.

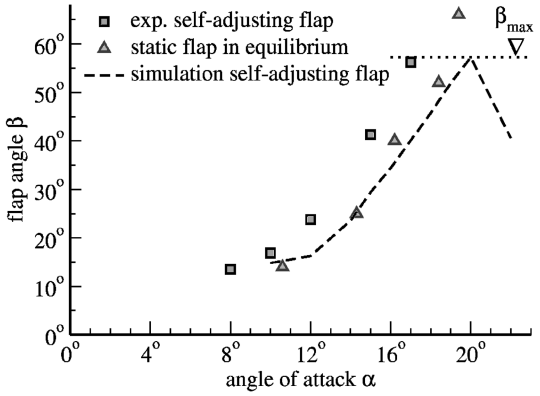

Fig. 19 Deflection of a self-adjusting flap in comparison to a static flap in equilibrium position and to experiments.

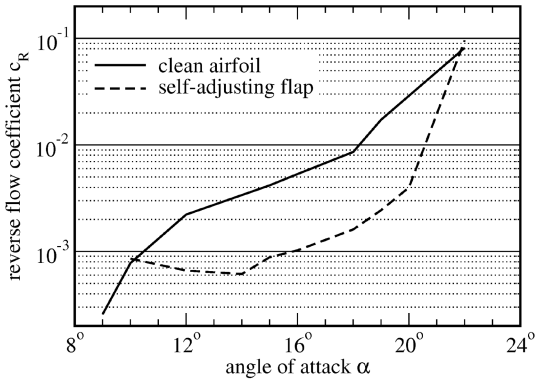

Fig. 20 Reverse flow coefficient c_R at $x/c = 0.99$ for the self-adjusting flap compared to the clean reference airfoil.

Comparison of experiments and numerical simulations in the predicted pressure distribution at $\alpha = 18$ deg angle of attack are shown in Fig. 21. Again the prediction of delayed separation for the clean configuration in the same simulation ($x/c = 0.55$) compared to the experiments ($x/c = 0.35$) becomes obvious. Although the differences between experiment and numerical simulation remain minor, a shift in the pressure between the upper and the lower surface of the flap is clearly visible. As a consequence, the flow on the upper surface is able to remain attached for a longer range of chord. Part of the lift is generated by slightly higher pressure on the lower surface which can be observed in both figures.

The interaction of movable flaps on a swept wing has been investigated by Meyer [6]. For swept wings, the occurring crossflow dominates the stall behavior and interacts with the reverse flow responsible for the opening of the flap. The movable flap is only able to block the separated flow in a forward direction. Consequently, self-adjusting flaps are not able to provide satisfactory performance on swept wings [6].

4. *Influence of Flap Mass*

The equilibrium position, however, does not provide the maximum achievable lift. Lower flap angles result in higher efficiency. Flaps with increased mass move to a lower flap deflection under gravity. This small β has a beneficial effect on the mean lift which can be enhanced by 15.3% as opposed to 12.9% from a tripled mass flap (Figs. 22 and 23). Unfortunately, in the experiments it became clear that excessively heavy flaps inhibit the automatic opening mechanism. Instead of an increased mass a similar effect, however, could be obtained by a torsion spring that behaves comparable to real bird feathers.

IV. Flight Experiments with Movable Flaps

After wind tunnel testing and theoretical analysis, self-adjusting flaps were installed on an aircraft for free flight tests [5,6]. The

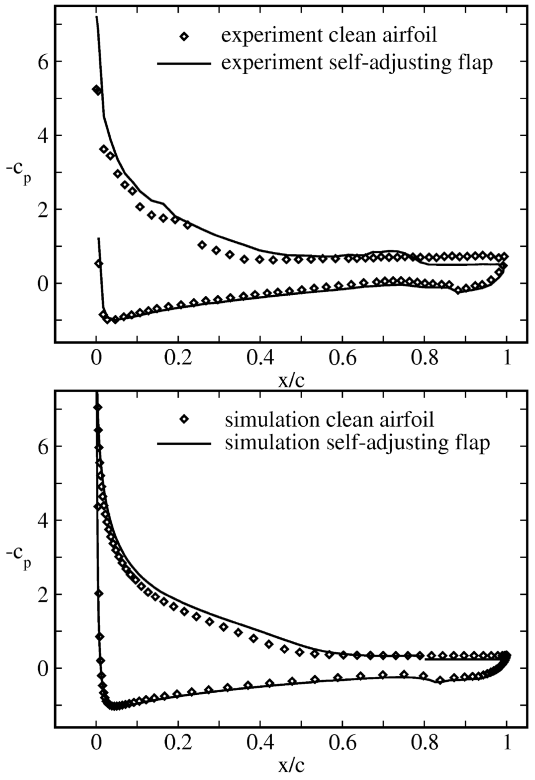

Fig. 21 Pressure distribution on the airfoil at $\alpha = 18$ deg with and without movable flap. Upper figure: experimental data; lower figure: computational results.

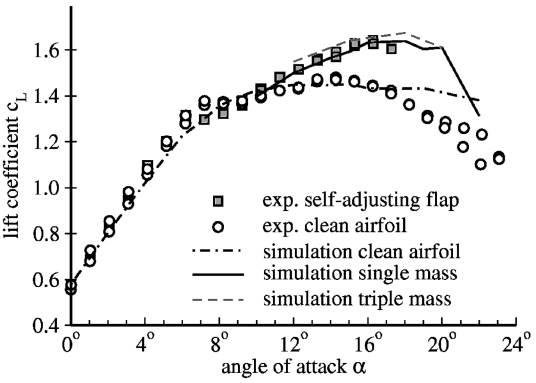

Fig. 22 Lift coefficient of an airfoil with free-movable flaps of different mass.

aircraft available for the experiments was a STEMME S10 motor glider. Using its piston engine, it can take off unassisted and the foldable propeller can be retracted into the nose of the cockpit. During flight, the motor can be restarted if necessary. With retracted propeller, the aircraft is a fast high-performance glider. The laminar wing is equipped with conventional flaps which also function as ailerons. The HQ41 airfoil cross section deviates only minimally on the rear part of the pressure side from the HQ17 (Fig. 3) whose coordinates are given in a description of the experiments [4]. As a specific preparation for flight experiments with this aircraft, it was assured that the movable flaps would also work properly in combination with the conventional flaps on the wings.

Figure 5 shows data with both types of flaps combined. The movable flap is actually mounted on the conventional flap. As can be seen, the increase of lift caused by the movable flap is reproduced. During the flight experiments, the intention was to fly at very high angles of attack encroaching on the regime of total stall. Usually, for tests of high-lift systems, one does not go so far to avoid dangerous situations such as spinning of the aircraft. These flight tests, however,

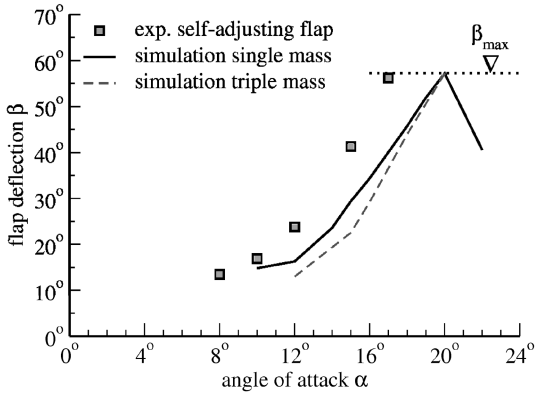

Fig. 23 Mean flap deflection β of free-movable flaps with varying mass.

included such situations with the purpose of demonstrating the inherent safety of the movable flaps. This required the following:

1) a very skilled pilot, well familiar with the behavior of the aircraft,

2) sufficient altitude during critical flight phases to have sufficient time available for the pilot to handle the arising situations, or in the worst case (which did not occur), to bail out,

3) the introduction of the attitude changes in a gradual stepwise fashion to avoid unfamiliar situations for the pilot,

4) a "special preparation" of the aircraft to keep it controllable.

The latter special preparation can be seen in Fig. 24. The elevator was equipped with vortex generators on the upper surface in order to extend its angular regime of attached flow. The same vortex generators were installed on the outer parts of the wings. This caused an increase of maximum lift of 31%. However, some peculiar flight-dynamical effects were caused by this: the return to normal flight attitude from the stall-spinning sequence sometimes resulted in spin in the opposite direction. This was probably caused by the exaggerated asymmetry in lift between attached and fully separated flow conditions on the outer wing, due to the vortex generators.

A reduction to half the previous number of the vortex generators (i.e., a reduced vortex generator density) reduced the increase of maximum lift to merely 15% on the outer wings. This turned out to be more compatible with the original flight-dynamical layout of the aircraft and thereby eliminated the problem. In addition, the performance of the outboard wing section then became closer to the inboard section with movable flaps. Incidentally, for the solution of these safety-relevant problems it proved very useful that the full-scale wind tunnel experiment was available in parallel to the flight tests. To highlight the flow situation on the wing, woolen tufts were attached to its surface.

These and the motion of the movable flaps were recorded by a video camera on the empennage. On the video tape the flight speed was also recorded. Typical flow situations can be seen in Fig. 25. The video pictures in Fig. 25 are fully consistent with parallel experiments in the wind tunnel at identical air speed and Reynolds number. In flight experiments, the increase in maximum lift coefficient c_L can be documented by recording the minimum

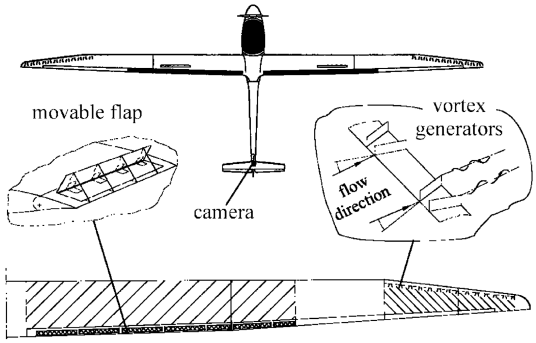

Fig. 24 STEMME S10 test aircraft, equipped with movable flaps and vortex generators.

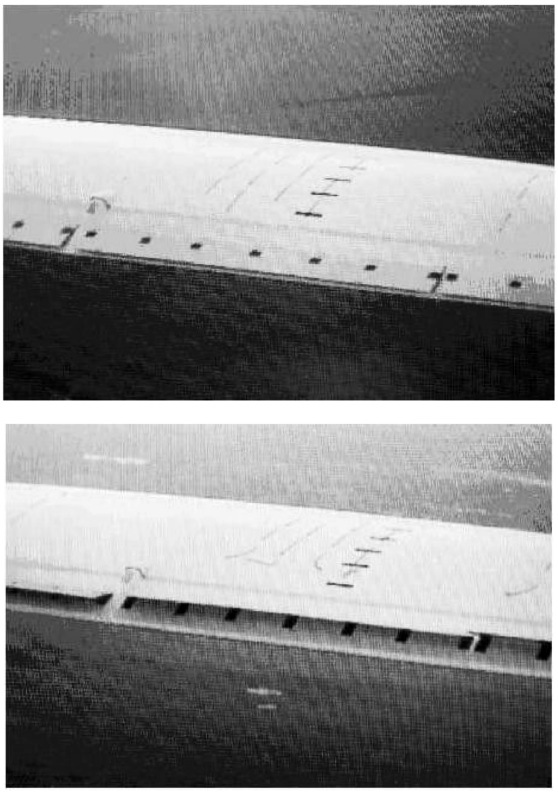

Fig. 25 In-flight video recording. The upper picture shows attached flap and attached flow. On the lower picture, the woolen threads indicate partial separation and the movable flap has risen by itself.

attainable speed before stall. Therefore, during the tests, the flight speed had been reduced very gradually until total stall occurred. The reduction in minimum speed due to the movable flaps was recorded in this way. For comparison, test flights were also carried out where the movable flaps had been locked. The reduction in minimum speed due to the movable flaps was 3.5%. Considering the actual aircraft weight in the moment in which the stall occurs that corresponds to a 7% increase of lift. Taking into account that only 61% of the wing area was equipped with movable flaps (Fig. 24), one obtains an 11.4% increase of maximum lift for the airfoil. This is almost exactly the same value that had been obtained previously in the wind tunnel and by the numerical simulation with the same movable flap [4,16].

The comments of the pilot were also positive. Permanent spinning did not occur following a straight-flight stall situation. By contrast, with locked movable flaps, permanent spinning did develop from the same situation. However, due to our cautiousness, the flaps were only installed in the inner part of the wing. Therefore, the changes in flight behavior were only moderate, albeit positive. Another observation was that keeping the flight speed at low and near-stall values appeared to be easier with movable flaps. More detailed information can be found in a report on this subject [16].

V. Summary

The effect of self-adjusting movable flaps on airfoils similar to the outer layer of feathers on the upper surface of bird wings has been demonstrated in experimental and numerical investigations. It has been shown that lift can be enhanced by more than 10%. The main effect of the flap can be described as a blockage of the reverse flow from the trailing edge region to the suction peak resulting in a delayed flow separation.

This simple and cost-effective flow control tool can be combined with other devices. Its performance has already been demonstrated in free-flight experiments with a glider airplane. The application is, however, limited to subsonic flows and nonswept wing configuration.

Acknowledgements

This research is funded by the German Research Foundation (DFG) under the umbrella of the Collaborative Research Center (Sonderforschungsbereich, Sfb 557, "Beeinflussung komplexer turbulenter Scherstroemungen") at the Technical University Berlin. The person who took the highest personal risk in this project was the test pilot P. Montag of the STEMME Aircraft Company, Strausberg. In addition, we appreciate the support of R. Stemme and M. Lang of this company. A test wing was supplied by A. Quast, DLR Braunschweig. Financial support was supplied by the Volkswagen-Stiftung and the German Federal Ministry of Science, Technology and Education (BMBF) and is gratefully acknowledged. Very valuable comments and advice were provided by W. Liebe, Berlin and J. Mertens, DaimlerChrysler Aerospace Airbus GmbH, Bremen.

References

[1] Liebe, W., "Der Auftrieb am Tragflügel: Entstehung und Zusammenbruch," *Aerokurier*, Vol. 12, No. 12, 1979, pp. 1520–1523.

[2] Malzbender, B., Projekte der FV Aachen, "Erfolge im Motor- und Segelflug," *Aerokurier*, Vol. 1, No. 01, 1984.

[3] Patone, G., and Mueller, W., "Aeroflexible Oberflächenklappen als "Rückstrombremsen" nach dem Vorbild der Deckfedern des Vogelflügels," Technische Universität TR-96-05, Berlin, 1996.

[4] Bechert, D. W., Bruse, M., Meyer, R., and Hage, W., "Biological Surfaces and Their Technological Application—Laboratory and Flight Experiments on Drag Reduction and Separation Control," AIAA Paper 97-1960, 1997.

[5] Bechert, D. W., Bruse, M., Hage, W., and Meyer, R., "Review Article: Fluid Mechanics of Biological Surfaces And Their Technological Application," *Naturwissenschaften*, Springer, New York, Vol. 87, 2000, pp. 157–171.

[6] Meyer, R. K. J., "Experimentelle Untersuchungen von Rückstromklappen auf Tragflügeln zur Beeinflussung von Strömungsablösung," Ph.D. Thesis, Technische Universität Berlin, Mensch & Buch Verlag, Berlin, 2000.

[7] Parkinson, G. V., Brown, G. P., and Jandali, T., "The Aerodynamics of Two-Dimensional Airfoils with Spoiler. In V/STOL Aerodynamics," AGARD CP-143, pp. 14/1–14/10, Elsevier, Amsterdam, 1974.

[8] Horstmann, K. H., and Quast, A., "Widerstandsverminderung durch Blasturbulatoren," DFVLR, TR FB81-33, 1981.

[9] Rung, T., and Thiele, F., "Computational Modelling of Complex Boundary-Layer Flows," *Proceedings of the 9th International Symposium on Transport Phenomena in Thermal-Fluid Engineering*, Singapore, 1996.

[10] Schatz, M., "Numerische Simulation der Beeinflussung Instationärer Strömungsablösung durch frei Bewegliche Rückstromklappen auf Tragflügeln," Ph.D. Thesis, Technische Universität Berlin, Mensch & Buch Verlag, Berlin, 2003.

[11] Spalart, P. R., Shur, M., Strelets, M., and Travin, A., "Detached-Eddy Simulation of an Airfoil at High Angle of Attack," *Engineering Turbulence Modelling and Experiments*, Elsevier, Amsterdam, Vol. 4, 1999.

[12] Strelets, M., "Detached-Eddy Simulation of Massively Separated Flows," AIAA Paper 2001-0879, 2001.

[13] Wick, A., "A Novel Method for Generation of Dynamic Meshes," *Proceedings of the 7th International Conference on Numerical Grid Generation in Computational Field Simulations*, Whistler, Canada, 2000.

[14] Anderson, E. A., and Szewczyk, A. A., "Effects of a Splitter Plate on the Near Wake of a Circular Cylinder in 2- and 3-Dimensional Flow Configurations," *Experiments in Fluids*, Vol. 23, No. 23, 1997, pp. 161–174.

[15] Bearman, P. W., "Investigation of the Flow Behind a Two-Dimensional Model with a Blunt Trailing Edge and Fitted with Splitter Plates," *Journal of Fluid Mechanics*, Vol. 21, No. 21, 1965, pp. 241–255.

[16] Meyer, R., Bechert, D. W., Hage, D. W., and Montag, P., "Aeroflexible Oberflächenklappen als Rückstrombremsen nach dem Vorbild der Deckfedern des Vogelflügels," DLR IB92517-96/B5, 1997.

M. Ahmadian
Associate Editor